Contrib Mineral Petrol (1992) 110:121–132

Contributions to Mineralogy and Petrology

Phase relationships in Buchan facies series pelitic assemblages: calculations with application to andalusite-staurolite parageneses in the Mount Lofty Ranges, South Australia

Peter Dymoke and Michael Sandiford

Department of Geology and Geophysics, University of Adelaide, G.P.O. Box 498, SA 5001, Australia

Received March 15, 1991 / Accepted October 2, 1991

Abstract. Low-pressure, medium- to high-temperature (Buchan-type) regional metamorphism of pelitic rocks in the Mount Lofty Ranges, South Australia, is defined by the development of biotite, staurolite-andalusite, fibrolite, prismatic sillimanite and migmatite zones. K-feldspar makes its first appearance in the prismatic sillimanite zone and here we restrict our discussion to lower grade assemblages containing prograde muscovite, concentrating particularly on well-developed andalusite-staurolite parageneses. In general, the spatial distribution and mineral chemical variation of these assemblages accord with the predictions of petrogenetic grids and P–T and T–X_{Fe} pseudo-sections constructed from the internally consistent data set of Holland and Powell (1990) in the system KFMASH, assuming $a(H_2O) \sim 1$, although analysed white mica compositions are systematically more aluminous than predicted. Importantly, the stability ranges of most critical assemblages predicted by these grids and pseudo-sections coincide closely with P–T estimates calculated using the data set of Holland and Powell (1990) from the Mount Lofty Ranges assemblages. With the exception of Mn in garnet and Zn in one staurolite-cordierite-muscovite assemblage non-KFMASH components do not significantly appear to have affected the stability ranges of the observed assemblages. An apparent local reversal in isograd zonation in which andalusite first appears down-grade of staurolite suggests a metamorphic field gradient concave towards the temperature axis and, together with evidence for essentially isobaric heating of individual rocks, is consistent with the exposures representing an oblique profile through a terrain in which heat was dissipated from intrusive bodies at discrete structural levels.

Mineral abbreviations used in figures

als	Al_2SiO_5 phase	and	andalusite
bi	biotite	cd	cordierite
chl	chlorite	gt	garnet
ky	kyanite	mu	muscovite
ph	phengite	q	quartz
sill	sillimanite	st	staurolite

Introduction

The pressure–temperature (P–T) conditions of equilibration of metamorphic rocks commonly testify to the existence of extremely perturbed thermal regimes in orogenic zones. In order to understand the processes responsible for these thermal perturbations it is necessary to obtain precise constraints on the spatial and temporal variations in pressure and temperature. Due to our increasing knowledge of the thermodynamic properties of the common rock-forming minerals, the P–T evolution of metamorphic terrains now can be constrained in a variety of ways. However, the constraints remain imperfect and many conventional geothermobarometric techniques are subject to well-recognised and often large errors due to poorly constrained activity models for crucial phases as well as analytical errors (see Powell 1985; Essene 1989; Holland and Powell 1990 for further discussion). In addition, it is often difficult to decide objectively on the suitability of a given calibration without assessing its results, thus introducing circularity. These problems can be reduced, though not entirely removed, by use of an internally consistent thermodynamic data set to calculate the P–T conditions of equilibration of specific, widely distributed, low-variance mineral assemblages. One advantage of this approach is that the variation in P–T conditions across the terrain can be assessed without the need for absolute P–T values.

Comprehensive data sets, such as that of Holland and Powell (1990), containing data for mineral end-members related by the Fe Mg_{-1} and the (Mg,Fe)$SiAl_{-2}$ (Tschermak's) exchanges common to metamorphic minerals allow evaluation of several independent equilibrium relations for individual assemblages (see Holland and Powell 1990; Guiraud et al. 1990; Will et al. 1990). For example, the data set of Holland and Powell (1990) contains data for 15 end-members for the assemblage

muscovite + biotite + chlorite + garnet + quartz + fluid, allowing 9 independent constraints to evaluate P–T–X relations. More importantly, as shwon by Powell and Holland (1990) for pelites and Guiraud et al. (1990) and Will et al. (1990) for mafic and ultramafic compositions, such data sets allow comprehensive evaluation of the reaction space of individual bulk-rock compositions. However, it remains important to test predictions of such data sets with appropriate natural occurrences. In this paper we use the Holland and Powell (1990) data set to calculate the P–T–X evolution of low P pelites appropriate to "Buchan" zones, expanding upon the results of Powell and Holland (1990), and comparing the results with assemblage variations in a low-pressure regional metamorphic terrain in the Mount Lofty Ranges, South Australia. We are primarily concerned with P–T significance of the andalusite-staurolite zone which is particularly well developed in the Mount Lofty Ranges.

Low-P metamorphism in the Mount Lofty Ranges

The Mount Lofty Ranges, South Australia, form the southern portion of the Adelaide Fold Belt (Fig. 1) which extends from Kangaroo Island in the south to the Flinders Ranges in the north. This fold belt consists of late Proterozoic "Adelaidean" sediments, overlain by, and probably partly in fault contact with, the Lower Cambrian Normanville and Kanmantoo groups (Daily and Milnes 1972). These two groups comprise a varied sequence of clastics, carbonates and volcanic horizons (Milnes 1982). All the metamorphic assemblages discussed here occur in the Kanmantoo group. These sedimentary sequences were deformed and metamorphosed during the late Cambrian to early Ordovician Delamerian Orogeny (e.g. Glen et al. 1977). Metamorphism is usually low-grade, but medium- to high-grade, low-pressure metamorphism occurs mainly in the Kanmantoo Group sediments, with migmatite zones being developed about syn-orogenic acid plutons. The metamorphic peak is closely associated with second-generation structures (D_2): field observations suggest that migmatisation occurs before and during F_2 folding, while at lower grades, staurolite and andalusite porphyroblasts overgrow developing S_2 crenulations. It appears therefore that the lower grade exposures attained peak temperatures later than higher grade regions, suggesting a significant lateral heat transfer outward from the zone of plutonism.

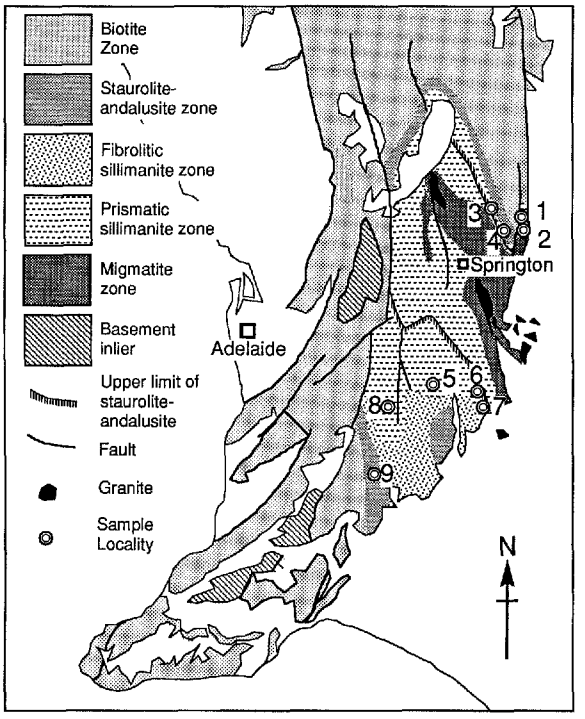

Fig. 1. Geological map of the Adelaide Fold Belt (isograd mapping after Offler and Fleming 1968 and Mancktelow 1990) showing the regional metamorphic zonation of the Mount Lofty Ranges terrain and the localities of samples used for pressure-temperature estimates (see text). Sample localities are *1*, 185–440; *2*, 185–829; *3*, 185–716; *4*, 185–636/4; *5*, A281 series; *6*, 474–318; *7*, 474–333, a, b; *8*, 474–428; *9*, 890–111

Table 1. Phengite (white mica) analyses used in P–T estimates from Mount Lofty Ranges assemblages (recalculated to 11 oxygens)

	185-636/4	474-333	474-333A	474-333B	474-428	A281-215	A281-223	A281-716	890-111
SiO_2	46.58	45.52	46.09	45.88	44.80	46.06	46.23	45.88	46.51
TiO_2	0.25	0.14	0.73	0.54	0.46	0.28	0.36	0.21	0.78
Al_2O_3	38.30	37.74	37.46	37.39	35.85	37.45	38.47	38.08	36.78
FeO	0.88	0.50	0.71	0.76	2.19	1.49	1.00	1.60	0.56
MgO	0.51	0.56	0.58	0.54	0.50	0.44	0.32	0.37	0.53
Na_2O	1.40	1.14	1.03	1.02	1.36	0.88	1.73	1.79	1.01
K_2O	9.52	9.90	10.10	9.93	9.64	9.34	8.73	8.17	9.56
Total	97.4	95.5	96.7	96.1	94.8	95.9	96.8	96.1	95.7
Si	3.011	3.004	3.010	3.014	3.010	3.025	2.999	3.000	3.053
Ti	0.012	0.007	0.036	0.027	0.023	0.014	0.018	0.010	0.039
Al	2.918	2.937	2.884	2.896	2.839	2.900	2.942	2.935	2.846
Fe^{2+}	0.048	0.028	0.039	0.042	0.123	0.082	0.054	0.087	0.031
Mg	0.049	0.055	0.056	0.053	0.050	0.043	0.031	0.036	0.052
Na	0.175	0.146	0.130	0.130	0.177	0.112	0.218	0.227	0.129
K	0.785	0.834	0.842	0.832	0.826	0.783	0.722	0.681	0.801
Total	6.998	7.011	6.998	6.993	7.049	6.958	6.983	6.997	6.95
$2X_{Al,T2}$	0.9894	0.9956	0.9898	0.9862	0.9902	0.9748	1.0014	1.0005	0.9469

Table 2. Biotite analyses used in *P–T* estimates from Mount Lofty Ranges assemblages (recalculated to 11 oxygens)

	185-636/4	185-716	474-318	474-333	474-333B	474-428	A281-215	A281-222	A281-223	A281-715	A281-716	890-111
SiO_2	34.85	35.94	35.05	34.81	35.17	35.17	33.94	35.01	34.38	35.50	34.20	35.07
TiO_2	1.20	1.55	1.21	2.08	1.80	1.34	2.00	1.67	1.77	1.83	1.66	1.45
Al_2O_3	19.41	19.70	19.35	19.10	19.63	19.02	19.60	19.71	19.63	19.83	19.75	19.53
FeO	18.66	17.29	20.03	18.62	18.63	18.76	23.62	19.98	21.42	22.77	22.13	18.99
MgO	9.78	10.84	9.60	9.70	9.97	10.25	6.20	8.16	8.03	7.95	8.52	8.78
Na_2O	0.44	0.44	0.14	0.17	0.24	0.65	0.40	0.55	0.50	0.62	0.48	0.41
K_2O	8.79	9.23	9.41	8.88	8.89	9.19	9.19	9.04	8.77	9.06	8.63	8.79
Total	93.1	95.0	94.8	93.4	90.3	94.4	95.0	94.1	94.5	97.6	95.4	93.0
Si	2.699	2.708	2.690	2.686	2.682	2.697	2.652	2.701	2.661	2.673	2.631	2.720
Ti	0.070	0.088	0.070	0.121	0.103	0.077	0.118	0.097	0.103	0.104	0.096	0.085
Al	1.772	1.750	1.751	1.737	1.765	1.719	1.805	1.793	1.792	1.760	1.791	1.786
Fe^{2+}	1.209	1.090	1.286	1.201	1.188	1.203	1.543	1.289	1.387	1.434	1.424	1.232
Mg	1.129	1.217	1.098	1.115	1.133	1.171	0.722	0.938	0.926	0.892	0.977	1.015
Na	0.066	0.064	0.021	0.025	0.035	0.097	0.061	0.082	0.075	0.091	0.072	0.062
K	0.868	0.887	0.921	0.874	0.865	0.899	0.916	0.890	0.866	0.870	0.847	0.870
Total	7.828	7.805	7.836	7.760	7.771	7.864	7.816	7.791	7.81	7.824	7.837	7.768
$2X_{AlM2}$	0.42	0.46	0.44	0.42	0.45	0.42	0.46	0.49	0.45	0.52	0.42	0.51

Migmatite, primsatic sillimanite, fibrolite, andalusite+staurolite, and biotite zones (defined by first appearances) are arranged about a zone of plutons (Mills 1964; Offler and Fleming 1968; Mancktelow 1990; Fig. 1). K-feldspar makes its first appearance in the prismatic sillimanite zone. Mills (1964) has mapped separate andalusite and staurolite isograds north-east of Springton (see Fig. 1), staurolite generally appearing down-grade of andalusite (see also Sandiford et al. 1990). However, near the eastern margin of the exposed terrain, the andalusite and staurolite isograds apparently cross each other, such that staurolite appears first up-grade of andalusite (Mills 1964; Offler and Fleming 1968). Down-grade of the the first appearance of K-feldspar, the common pelitic assemblages in this terrain are combinations of the following phases:

biotite + quartz + plagioclase + ilmenite ± muscovite ± andalusite ± sillimanite ± staurolite ± garnet.

Chloritoid has not been recorded. In this contribution we consider explicitly those assemblages with quartz + biotite + muscovite and which therefore are treated, with the fluid phase, as excess phases in the calculated phase relations discussed below, although we emphasise that not all pelitic rocks of appropriate grade contain muscovite. In the sequence of assemblages preserved in the field, the first appearance of andalusite + staurolite coincides with the disappearance of primary chlorite (Mills 1964; Offler and Flemig 1968) while the first appearance of prismatic sillimanite as mapped by Mancktelow (1990) and shown on Fig. 1 occurs before the disappearance of andalusite and staurolite (note that this contrasts with Offler and Fleming 1968, who considered the sillimanite grade to be considerably more restricted than shown in Fig. 1). Fibrolite is commonly present in andalusite-bearing assemblages. This distribution of fibrolite, down-grade of prismatic sillimanite, mirrors that described in a contact aureole in the Irish Dalradian by Kerrick (1987), who suggested that this fibrolite formed metastably in the andalusite *P–T* stability field.

Sandiford et al. (1990) have documented textural evidence for the breakdown of staurolite to cordierite in a muscovite-bearing assemblage in the Springton region, near the eastern margin of the present exposure. They argued from qualitative phase constraints based on the petrogenetic grid of Harte and Hudson (1979) that reaction occurred during significant approximately isobaric heating. Further evidence for approximately isobaric heating at this time comes from the close association of this reaction with the transition of andalusite to fibrous sillimanite, while elsewhere in the Springton region, relict kyanite is armoured by andalusite and sillimanite, also indicating approximately isobaric heating. In addition, Arnold and Sandiford (1990) have documented reactions involving the metasomatic removal of K_2O during essentially isobaric prograde heating, resulting in the breakdown of staurolite + biotite and aluminosilicate + biotite to cordierite + orthoamphibole.

Representative mineral analyses from pelitic assemblages within the staurolite-andalusite and sillimanite zones are shown in Tables 1–4. Note that garnets coexisting with staurolite and andalusite (as well biotite, muscovite and quartz) contain appreciable spessartine component (Table 4).

Calculated phase equilibria

Here, we present a calculated petrogenetic grid and calculated *P–T* and T–X_{Fe} pseudo-sections (see Hensen 1971; Hudson 1980) for the assemblage chlorite, aluminosilicate, staurolite, cordierite and/or garnet with biotite + muscovite + quartz + H_2O in excess in the system KFMASH. These grids and pseudo-sections were generated with the data set of Holland and Powell (1990), and version 2b1 of the computer program Thermocalc (see also Guiraud et al. 1990; Powell and Holland 1988, 1990).

Table 3. Staurolite analyses used in *P–T* estimates from Mount Lofty Ranges assemblages (recalculated to 48 oxygens)

	474-318	474-428	185-636/4	185-716	A281-716	A281-215	A281-222	A281-223	A281-715
SiO_2	24.84	25.35	25.76	25.00	24.86	25.00	24.41	25.71	25.90
TiO_2	0.71	0.55	0.39	0.51	0.50	0.28	0.41	0.45	0.33
Al_2O_3	56.10	55.03	54.95	55.60	54.66	56.27	53.73	56.17	56.35
FeO	14.25	13.93	12.41	13.88	15.44	14.79	14.76	15.01	14.56
MnO	0.30	0.64	0.40	0.30	0.21			0.15	
MgO	1.79	1.85	1.59	1.64	1.64	1.21	1.32	1.50	1.47
Total	98.0	97.4	95.5	96.9	97.3	97.8	95.0	99.4	98.6
Si	7.222	7.387	7.552	7.324	7.322	7.300	7.367	7.400	7.453
Ti	0.155	0.121	0.086	0.112	0.111	0.061	0.093	0.097	0.071
Al	19.228	18.905	18.992	19.202	18.979	19.371	19.116	19.060	19.118
Fe^{2+}	3.465	3.395	3.043	3.401	3.803	3.612	3.725	3.613	3.504
Mn	0.074	0.158	0.099	0.074	0.052	0.000	0.000	0.037	0.000
Mg	0.776	0.803	0.695	0.716	0.720	0.527	0.594	0.643	0.630
Total	30.920	30.769	30.467	30.829	30.987	31.035	31.070	30.850	30.777

X_{Fe} relations among coexisting Fe-, Mg-bearing phases

The chemographic relations amongst coexisting ferromagnesian phases as predicted by Thermocalc require some comment in as much as they have considerable bearing on the detailed reaction relationships in the KFMASH system. In general these predicted relationships correspond closely with the relationships found in nature (see Powell and Holland 1990), with two important possible exceptions. These are: (1) staurolite is slightly more Fe rich than coexisting garnet; (2) chlorite is less magnesian than cordierite and is less aluminous than the biotite-cordierite tieline in AFM (Al_2O_3, FeO, MgO triangle as projected from muscovite, quartz, and H_2O).

The predicted Fe–Mg partitioning between coexisting staurolite and garnet, namely $X_{Fe,st} > X_{Fe,gt}$, is inconsistent with the measured partitioning in the Mount Lofty Ranges assemblages (see below) and is contrary to common, but by no means all, experience (see for example discussion by Grew and Sandiford 1985). An important implication of this is that the reaction (cordierite, chlorite) produces prograde muscovite (in accordance with convention invariant assemblages are designated by the absent phases in square brackets while univariant assemblages by the absent phases in round brackets):

staurolite + biotite = garnet + aluminosilicate + muscovite (+ quartz, H_2O).

We regard this prediction as incorrect, but as discussed by Powell and Holland (1990) the differences between $X_{Fe,st}$ and $X_{Fe,gt}$ are very slight and within error the calculated Fe–Mg relationships between the two phases may be reversed, giving rise to the expected reaction relationship:

staurolite + muscovite
= garnet + aluminosilicate + biotite (+ quartz, H_2O).

Apart from the reaction relationships about (cordierite, chlorite), the relative partitioning of Fe and Mg between garnet and staurolite does not affect the topology in any other way.

While there is general agreement that chlorite is less magnesian than cordierite the position of chlorite with respect to the biotite – cordierite tieline in AFM is contentious, in part due to the rarity of appropriate natural assemblages (see discussion by Harte and Hudson 1979; Hudson 1980). For example, the grids of Hess (1969) and Thompson (1976) are based on the assumption that chlorite compositions lie within the biotite-cordierite-aluminosilicate tie triangle, a conjecture for which some support is provided by the findings of Guidotti et al. (1975). In contrast, Harte and Hudson (1979) and Hudson (1980) have argued that Dalradian sequences are better interpreted as the consequence of the prograde reaction:

chlorite + aluminosilicate
= biotite + cordierite (+ muscovite, quartz, H_2O)

as predicted by Thermocalc. An important consequence of chlorite compositions lying beneath the biotite – cordierite tieline is that for Al-poor bulk compositions (in AFM) saturated in biotite (as considered here), the most magnesian bulk compositions will contain the assemblage chlorite-biotite-muscovite-quartz-H_2O.

Calculated P–T grid (Fig. 2)

A *P–T* grid for the phases aluminosilicate, staurolite, cordierite, garnet, chlorite, with biotite + quartz + muscovite + H_2O in excess is shown in Fig. 2. Note that this grid differs with that of Powell and Holland (1990) in as much as that andalusite + biotite assemblages are stable, due to the predicted stability of the two invariant points [chlorite] and [garnet] in the andalusite stability field. Using an earlier version of the dataset Powell and Holland (1990) suggested that andalusite + biotite-bearing assemblages are unstable in KFMASH, but may be

Table 4. Garnet analyses used in *P–T* estimates from Mount Lofty Ranges assemblages (recalculated to 12 oxygens)

	185-440	185-636/4	474-318	474-333	474-333A	474-333B	474-428	A281-215	A281-222	A281-223	A281-715	A281-716	890-111
SiO_2	36.83	37.29	37.21	36.92	37.20	37.34	37.18	37.08	36.73	37.20	38.50	36.75	37.66
Al_2O_3	21.15	21.48	21.32	21.07	21.16	21.63	21.18	20.53	20.67	21.46	21.72	20.88	21.05
FeO	35.83	31.47	34.49	28.24	28.38	28.03	29.11	39.26	35.23	34.83	36.61	35.19	33.54
MnO	0.42	7.76	6.23	10.34	10.24	10.41	9.91	1.14	3.15	4.78	3.32	5.16	4.90
MgO	3.85	2.59	2.37	2.18	2.46	2.06	2.47	1.75	2.28	2.41	2.55	2.00	2.01
CaO	1.21	1.21	0.12	1.80	1.85	1.76	1.65	0.59	1.47	1.04	1.01	0.59	1.88
Total	99.3	101.8	101.7	100.6	101.3	101.6	101.6	100.4	99.4	101.8	103.7	100.5	101.0
Si	2.972	2.971	2.973	2.974	2.971	2.977	2.964	3.008	2.994	2.963	2.996	2.980	3.012
Al	2.012	2.018	2.008	2.001	1.992	2.033	1.990	1.963	1.986	2.015	1.993	1.996	1.985
Fe^{2+}	2.418	2.097	2.305	1.903	1.896	1.869	1.941	2.663	2.402	2.320	2.383	2.386	2.243
Mn	0.029	0.524	0.422	0.706	0.693	0.703	0.669	0.078	0.217	0.322	0.219	0.354	0.332
Mg	0.463	0.308	0.282	0.262	0.293	0.245	0.293	0.212	0.277	0.286	0.296	0.242	0.240
Ca	0.105	0.103	0.010	0.155	0.158	0.150	0.141	0.051	0.123	0.089	0.084	0.051	0.161
Total	8.000	8.020	8.000	8.001	8.003	7.976	7.997	7.976	7.999	7.996	7.970	8.009	7.973

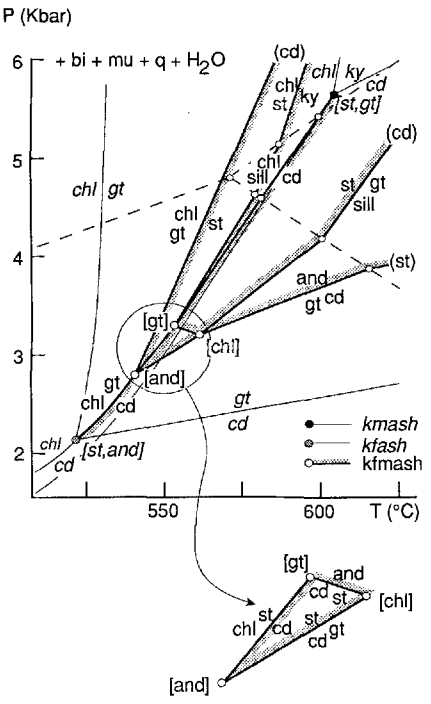

Fig. 2. Calculated *P–T* grid for reactions for the phases staurolite + cordierite + garnet + chlorite + andalusite + sillimanite + kyanite (biotite + muscovite + quartz + H_2O in excess) in the systems KFMASH, KFASH and KMASH. The *stippling* shows the side of the reactions on which biotite is produced, with muscovite on the opposite side

stabilized by increased $a(O_2)$ and/or TiO_2 increasing the area of the biotite stability field (see below).

The topology of our calculated *P–T* grid bears a remarkable similarity with the grid of Hess (1969) bearing in mind that some differences are necessitated by the disparate assumptions (see previous discussion) about the chemographic relations between: (1) staurolite and garnet [which alters the reaction relationships around (cordierite, chlorite)]; (2) chlorite, biotite and cordierite [which alters the reaction relationships around (staurolite, garnet)]. A notable similarity occurs in the restriction of stable cordierite + staurolite (+ biotite, muscovite, quartz, H_2O) to a small field bounded by [andalusite], [chlorite] and [garnet]. Our calculated grid restricts this possibility to pressures between 2.8 and 3.2 kbar and temperatures of 535–565° C, whereas the grid of Hess (1969) has this possibility at 2.7–4 kbar and 550–590° C. One important concern regarding the calculated topology shown in Fig. 2 as well as that of Hess (1969) is the predicted stability of the garnet-cordierite-muscovite assemblages (see also Powell and Holland 1990). As pointed out by Holdaway and Lee (1977) in the only known recorded occurrences of this assemblage the garnet contains appreciable Mn and/or Ca. Consequently, Holdaway and Lee (1977) and subsequently Harte and Hudson (1979) have considered garnet–cordierite–muscovite to be metastable as a basic assumption in building KFMASH grids. In their grids the KFMASH invariant points [andalusite] and [chlorite] are considered metastable with respect to the KFASH invariants [garnet,

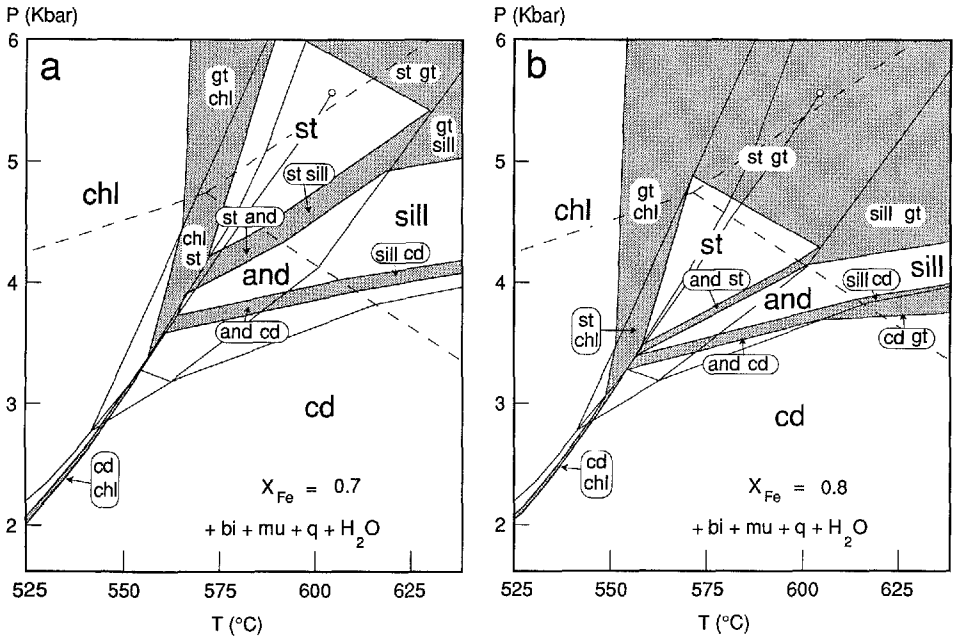

Fig. 3a, b. Calculated P–T pseudo-sections at constant X_{Fe} for the assemblage staurolite + cordierite + garnet + chlorite + andalusite + sillimanite + kyanite (biotite + muscovite + quartz + H_2O in excess) based on the P–T grid: **a** $X_{Fe}=0.7$; **b** $X_{Fe}=0.8$

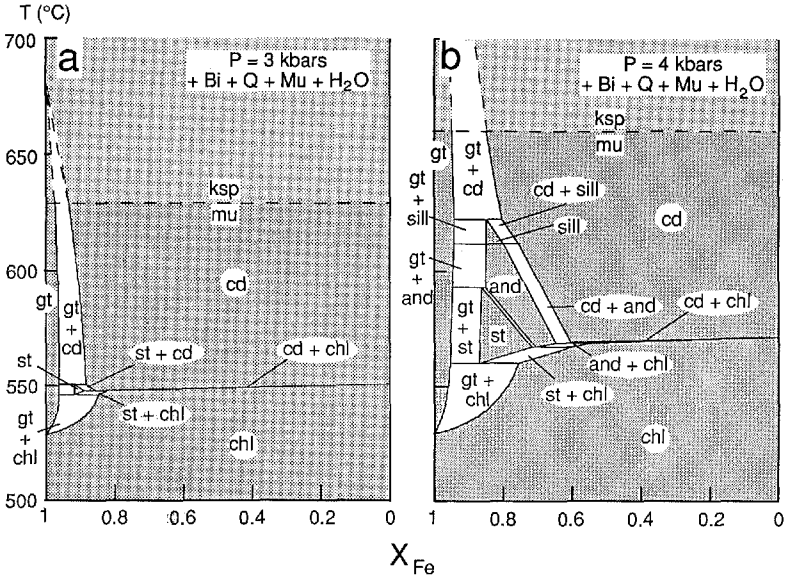

Fig. 4a, b. Calculated isobaric T–X_{Fe} pseudo-sections calculated from the P–T grid: **a** $P=3$ kbar; **b** 4 kbar. The *light stiple* and *dashed lines* in the high-temperature part of the sections signifies metastability of muscovite-quartz equilibria with regard to K-feldspar-bearing assemblages (e.g. Holdaway and Lee 1977)

andalusite] and [garnet, chlorite]. In defence of the calculated grid we note that while the association of garnet-cordierite-muscovite is predicted to be stable, the bulk compositional arguments presented below show that such an assemblage will be restricted to very narrow range of Fe-rich bulk compositions under a very restricted range of conditions at low P and high T (see also Figs. 3 and 4).

Calculated P–T pseudo-sections (Fig. 3)

Calculated P–T pseudosections for $X_{Fe}=0.7$ and 0.8 are presented in Fig. 3a, b. With biotite as an excess phase the compositional variation in this system effectively is given by the FM binary with garnet occuring in the most Fe-rich bulk compositions and chlorite in the most Mg-rich bulk compositions. The pseudo-sections are constructed for bulk compositions with Al contents slightly less than the garnet-chlorite join in AFM.

Despite substantial differences in the underlying P–T grids, the calculated pseudo-sections presented here are topologically equivalent to those of Hudson (1980), who derived his pseudo-sections from natural assemblages and the grid of Harte and Hudson (1979). This is because even for very Fe-rich ($X_{Fe}>0.8$) bulk compositions the [chlorite] invariant point is occluded by the cordierite (+muscovite, biotite, quartz, H_2O) stability field while the [andalusite] invariant point is occluded by the chlorite (+muscovite, biotite, quartz, H_2O) stability field (see Fig. 3b). In the pseudo-sections widespread stability of cordierite (+muscovite, biotite, quartz, H_2O) associa-

tion at low pressures for all bulk compositions restricts the association of garnet + cordierite (+ muscovite, biotite, quartz, H_2O) to a very narrow pressure window (~0.3 kbar) at about 3–3.5 kbar and temperatures near the upper stability of muscovite + quartz for bulk compositions more Fe-rich than $X_{Fe} = 0.8$ (see also Fig. 4). Consequently, this raises the possibility that the apparent absence of this natural garnet + cordierite (+ muscovite, biotite, quartz, H_2O) assemblage in systems approaching KFMASH may reflect the sensitivity of this association to bulk-rock composition rather than inherent metastability.

Calculated T–X_{Fe} pseudo-sections (Fig. 4)

Isobaric T-X_{Fe} pseudo-sections for pressures of 3 and 4 kbar are shown on Fig. 4. These pseudo-sections were constructed in a similar manner to the P–T pseudo-sections, using calculated garnet and chlorite compositions and the positions of staurolite, andalusite and cordierite derived projected onto the Fe–Mg binary from biotite, muscovite and quartz. The isobaric T–X_{Fe} pseudo-sections illustrate the dependence of stabilities of divariant assemblages on the bulk rock X_{Fe}. Note in particular the restriction of the staurolite-cordierite association to a very small range in X_{Fe} ~0.85–0.9 at 3 kbar and 545–550° C (Fig. 4a). The biotite zone is equivalent to the chlorite stability field on all the pseudo-sections, while the upper temperature limit to the andalusite − staurolite zone is represented by the upper temperature limit of the andalusite + staurolite stability field. The diagrams show how the staurolite + chlorite, andalusite + chlorite and cordierite + chlorite stability fields have very shallow T–X_{Fe} slopes, so that the dependence of the reactions involving those pairs of phases on bulk composition is weak. First-appearance isograds caused by these reactions are therefore good temperature indicators. In contrast, the andalusite + staurolite stability field has a steeper slope, so the isograd at which staurolite disappears makes a relatively poor isograd.

The Tschermak's exchange in sheet silicates (Fig. 5)

It is now well known that the compositions of end-members of many phases are related by the Tschermak's exchange, $Al_2(Fe,Mg)_{-1}Si_{-1}$. Since Thermocalc contains data for end-members whose compositions are related by this vector, it is possible to calculate the relationship between intensive variables and the extent of the Tschermak's exchange in given minerals (Powell and Holland 1990). For the assemblages considered here, the minerals in which the Tschermak's exchange occurs significantly are phengite (white mica), biotite and chlorite. Isopleths for $2X_{Al,M2,biotite}$, $X_{Al,M2,chlorite}$, and $2X_{Al,T2,muscovite}$ are shown superimposed onto our calculated P–T grid in Fig. 5a–c, respectively. In all three phases, Al contents increase with temperature at higher P and lower T than the KFMASH univariant reaction staurolite + chlorite = aluminosilicate. However, phengite and chlorite become Al-poorer with increasing temperature, while biotite Al contents are mostly pressure-sensitive at lower P and higher T than this reaction. In addition, compositions of all three phases are more sensitive to changing P–T at lower T and higher P than staurolite + chlorite = aluminosilicate, but less so at higher T and lower P. All three phases are predicted to be more Al-rich at lower pressures.

The predicted isopleths of phengite and biotite composition qualitatively agree closely with other theoretical and experimental constraints, most of which suggest increasing Al contents with higher temperature and lower pressure in low- to medium-grade pelitic assemblages

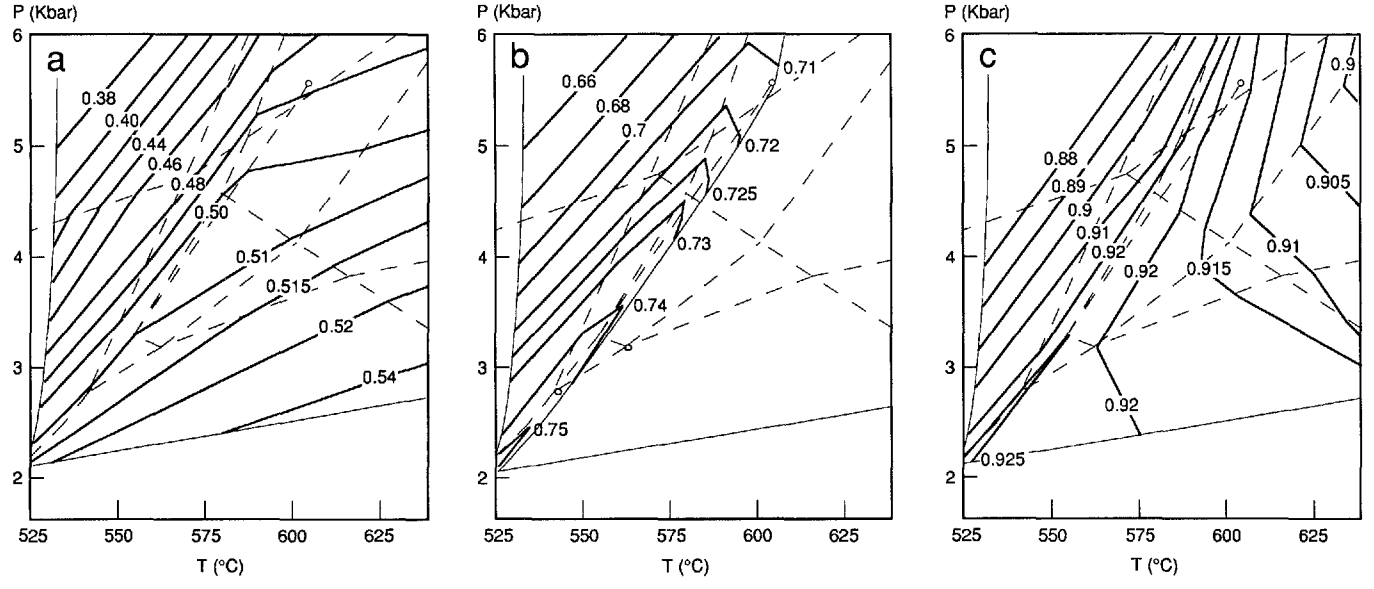

Fig. 5a–c. Calculated and extrapolated isopleths of sheet silicate compositions governed by the Tschermak's vector on the calculated P–T grid shown in Fig. 4; numbers on the contours are: **a** $2X_{Al,M2,biotite}$; **b** $X_{Al,M2,chlorite}$; **c** $2X_{Al,T2,muscovite}$

(e.g. Velde 1965; Powell and Evans 1983; Miyashiro and Shido 1984; Pattison 1987; Massonne and Schreyer 1987). In particular, based on the experimental data of Seifert (1970), Pattison (1987) showed that mica compositions along the KFASH or KMASH univariant reaction chlorite = cordierite (+biotite + quartz + muscovite + H_2O) become Si-richer with increasing temperature and pressure.

Effects of variable a(H_2O) (Fig. 6)

To assess the effect of variable a(H_2O), T–X_{Fe} sections have been generated with Thermocalc for $X(H_2O)$ values of 0.5 and 0.75 at $P = 4$ kbar (Fig. 6). These pseudo-sections show how the stability range of garnet and aluminosilicate are both increased at the expense of chlorite, cordierite and, to a lesser extent, staurolite, with the topology for unit water activity maintained to relatively low water activities. However, we note that the decrease in the temperature of the breakdown of muscovite + quartz to K-feldspar + sillimanite with decreasing a(H_2O) means that much of the calculated equilibria shown in Fig. 6 will be metastable (metastable portions of the muscovite-bearing equilibria are shown by dashed lines and light shading in Fig. 6).

Non-KFMASH components

In addition to KFMASH the phases discussed in the preceeding sections commonly contain appreciable amounts of other components, most notably TiO_2 and Fe_2O_3 in biotite, MnO in garnet and ZnO in staurolite. The effect of these non-KFMASH components on the topology of the grids is considered briefly in this section.

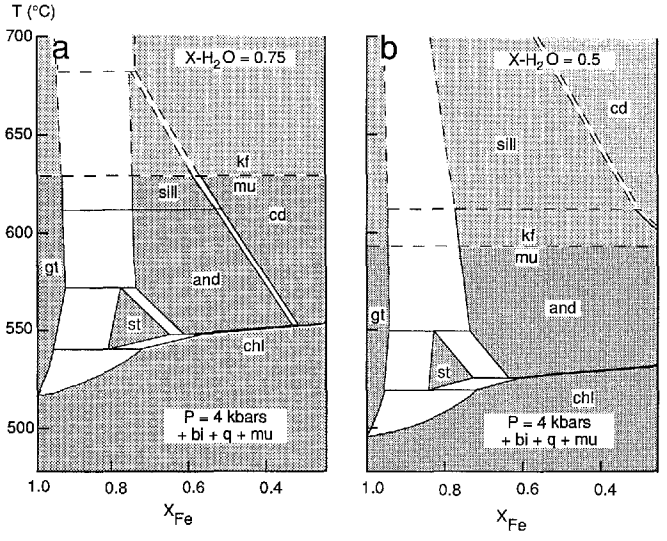

Fig. 6a, b. Quantitative T–X_{Fe} pseudo-sections for the assemblages calculated for $X_{H_2O} = 0.75$ and 0.5. Lowering X_{H_2O} causes the aluminosilicate and garnet stability fields to expand at the expense of chlorite, cordierite and staurolite. However, staurolite + chlorite continues to occur at lower temperatures than andalusite + chlorite. The *light stiple* and *dashed lines* in the high-temperature part of the sections signifies metastability of muscovite-quartz equilibria with regard to K-feldspar-bearing assemblages (e.g. Holdaway and Lee 1977)

Effect of TiO_2. Ilmenite is commonly present in the low-P pelitic assemblages allowing KFMASH-TiO_2 (KFMASHT) univariant reactions to be projected from ilmenite + biotite + muscovite + quartz + H_2O, generating a topologically equivalent grid to the KFMASH grid. As shown by Powell and Holland (1990), increasing TiO_2 with biotite in excess increases the stability ranges of the Al_2SiO_5 polymorphs to lower temperatures and pressures. In addition, the stability of cordierite at low pressures is increased to higher pressures at the expense of garnet. The staurolite stability range is also increased to lower temperatures and pressures at the expense of garnet. Note that the current thermodynamic data set predicts that andalusite + biotite-bearing assemblages are stable in the KFMASH system, in contrast to the earlier study of Powell and Holland (1990). As a result, it is no longer necessary to appeal to the existence of extra components such as TiO_2 for this association. We note that the effects of TiO_2 may be best assessed in terrains in which both cordierite and andalusite are part of the prograde sequence, that is at lower pressure than the Mount Lofty sequence (see below).

Effect of MnO. In the pelite system MnO is incorporated preferentially in garnet causing an expansion of all garnet-bearing stability fields with respect to KFMASH equivalents. Since no additional phase is stabilised by Mn, garnet-bearing KFMASH univariant curves become divariant in KFMASHMn. It seems likely that the KFMASHMn divariant equivalents to the KFMASH univariants connecting the intersections [andalusite] and [chlorite] are displaced towards [garnet], eventually "collapsing" the topology as Mn contents are increased. The stability field of garnet is thus increased to lower and higher pressures and temperatures at the expense of all other phases. In addition, the stability range of garnet + aluminosilicate is increased to higher pressures and lower temperatures. This collapse of the topology may have particularly dramatic effects on the stability of staurolite since its stability field in the KFMASH system forms a narrow sector bounded by garnet-producing reactions above ~3 kbar. With increasing Mn the low-P limit staurolite may be rapidly "squeezed" to higher pressures with the encroachment of the bounding garnet-producing reactions (divariant in KFMASHMn).

Effects of ZnO. Zirconium oxide preferentially is incorporated into staurolite, so staurolite stability ranges are increased with ZnO contents. As a result, the equivalents of the KFMASH [garnet] and [chlorite] are displaced to higher pressures and temperatures, while [andalusite] is displaced to lower pressures and temperatures. More importantly, the size of the cordierite + staurolite stability field is increased to higher pressures and temperatures, thus allowing a topology consistent with the replacement of staurolite by cordierite during dominantly isobaric

heating at pressures appropriate to the Mount Lofty Ranges sequence as discussed by Sandiford et al. (1990).

Comparison with Mount Lofty Ranges and other low-*P* sequences (Figs. 7 and 8)

The calculated pseudo-sections can be tested by: (1) whether they reproduce the progressive sequence of metamorphic zones accurately; (2) whether the predicted X_{Fe} values of the phases within a metamorphic zone are appropriate.

Harte and Hudson (1979) and Hudson (1980) provide detailed analysis of prograde metamorphic successions in the Buchan Zones in the Dalradian. Two distinct facies series are recognised, namely: the Ythan Valley Sequence (chlorite, cordierite-chlorite, andalusite-cordierite) and the Banffshire Coast Sequence (chlorite, cordierite-chlorite, andalusite-cordierite, staurolite-andalusite). Hudson (1980) recognises another distinct facies type in the Stonehaven Sequence (chlorite, garnet-chlorite, chlorite-staurolite and staurolite-garnet, sillimanite-staurolite). These sequences can be interpreted with regard to the calculated *P–T* pseudosections as shown in Fig. 7.

The sequence of assemblages outlined for the Mount Lofty Ranges resembles aspects of the the Stonehaven sequence, except for the absence of chloritoid and garnet zones immediately down-grade of the staurolite zone, as well as aspects of the Banffshire Coast Sequence from the Scottish Buchan Zones, except that staurolite typically occurs down-grade of andalusite and no distinct cordierite-muscovite zones are recognised. Though we have not calculated the stability ranges of chloritoid – bearing assemblages, these will probably lie in the lowest pressure parts of the garnet-chlorite two-phase field as shown in our grids (see also Harte and Hudson 1979; Powell and Holland 1990).

In low- to medium-grade pelitic assemblages, the most Fe-rich phase in three-AFM-phase assemblages is

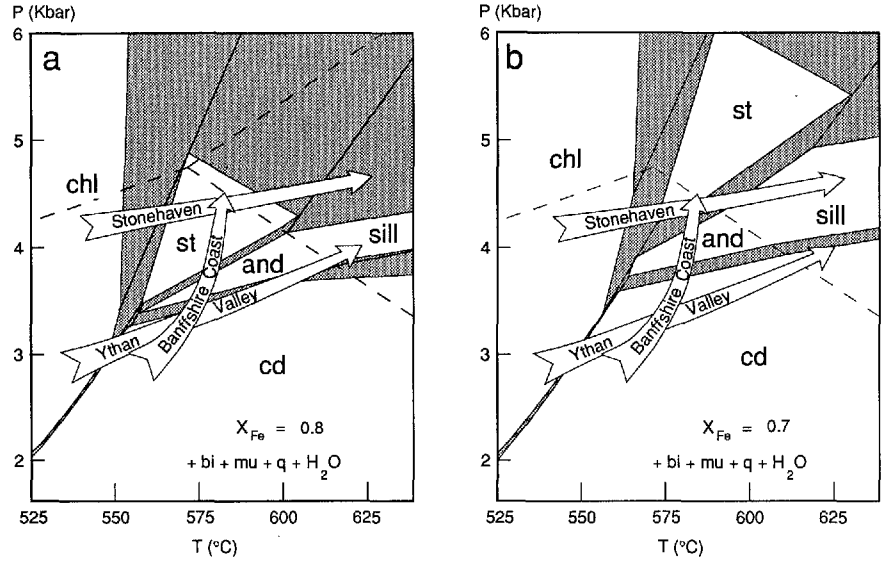

Fig. 7a, b. *P–T* pseudo-sections for X_{Fe} = 0.7 and 0.8 showing the zonal sequences and metamorphic-field gradients recognised in the the classic Buchan sequences documented by Harte and Hudson (1979) and Hudson (1980) in the Eastern Scottish Highlands

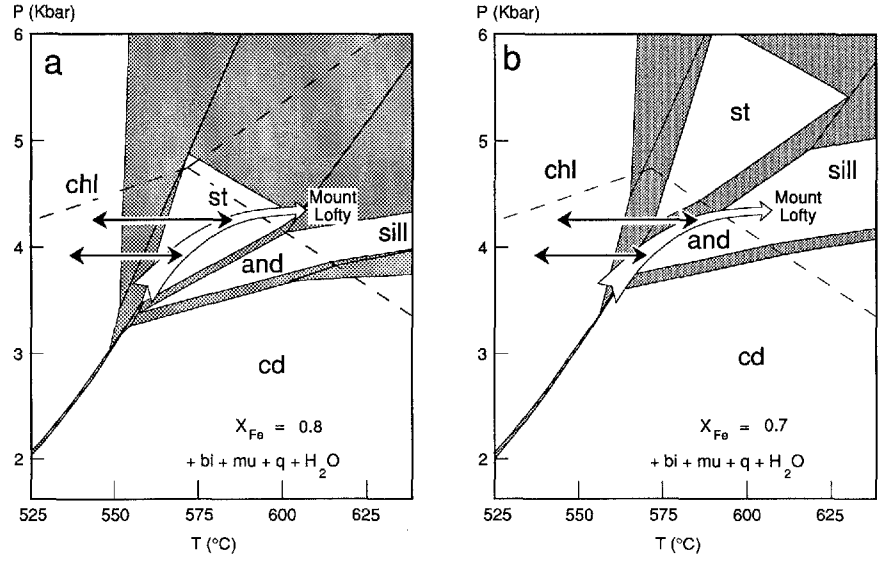

Fig. 8a, b. *P–T* pseudo-sections for X_{Fe} = 0.7 and 0.8 showing how the zonal sequences recognised in the Mount Lofty Ranges might be generated by an array of isobaric heating *P–T* paths, *double-headed black arrows*. These paths, in combination with an oblique exposed section through the terrain, *white broad curved arrow*, generate an andalusite isograd locally down-grade of the staurolite isograd

either staurolite or garnet. Note that the pseudo-sections reproduce the sequence of metamorphic zones in the Mount Lofty Ranges only for $X_{Fe} > 0.7$. The calculated pseudo-sections therefore predict that staurolite and garnet should have X_{Fe} values significantly greater than 0.7. As shown in Tables 3 and 4, typical X_{Fe} values for staurolite range between 0.8 and 0.85, while X_{Fe} for garnet ranges between 0.85 and 0.9. We note that, contrary to Thermocalc predictions, measured garnet is always more Fe-rich than staurolite in assemblages where both these phases are present.

For the 4–5 kbar and 550–650° C P–T conditions appropriate to the Mount Lofty Ranges assemblages (see below), predicted phengite compositions are very Al-rich with $2X_{Al,T2,muscovite}$ between 0.91 and 0.92 (3.08–3.09 Si per formula unit) while predicted biotite compositions are intermediate between phlogopite/annite and eastonite, giving $2X_{Al,M2,biotite}$ between 0.46 and 0.52. These predictions can be tested in the same way as the predicted X_{Fe} relations discussed above. Measured $X_{Al,M2,bt}$ values are between 0.42 and 0.56 (Table 1) and thus are comparable with the predictions. White micas in the Mount Lofty ranges assemblages have very high Al contents, with $2X_{Al,T2,muscovite}$ ranging between 0.96 and 0.99 (Table 2), and as such are enriched in Al with respect to predicted compositions. This discrepancy is not readily explained in mineral chemistry terms since the Mount Lofty Ranges phengites contain less than 0.1 wt% Fe_2O_3 and TiO_2, components which would otherwise increase the apparent Al/Si ratios in the phengites, and may imply that the assumption of ideal mixing is inappropriate. However, the calculated $2X_{Al,T2,muscovite}$ value is sensitive to the measured wt% SiO_2, with a change in SiO_2 by 1 wt% causing a change in $2X_{Al,T2,muscovite}$ of ca. 5%, and the discrepancy may reflect systematic errors in the measured Si contents in these minerals.

Many assemblages in the Mount Lofty Ranges bear garnet together with andalusite or staurolite as well as biotite, muscovite and quartz. As shown in Figs. 3 and 5, garnet is predicted to coexist with staurolite or sillimanite and at higher pressures and temperatures than the stability of andalusite + staurolite-bearing assemblages, except in very Fe-rich bulk compositions. The presence of garnet + andalusite assemblages at similar grades to garnet-absent assemblages therefore implies that significant bulk-rock Mn contents must have stabilised garnet in some assemblages, a suggestion supported by the often high Mn contents of the garnets in these assemblages (Table 4).

P–T conditions of metamorphism in the Mount Lofty Ranges

If the same internally consistent thermodynamic data set is used to calculate P–T conditions as well as a petrogenetic grid for a set of assemblages, close agreement between the grid and P–T estimates should be expected, unless there is strong petrological disequilibrium in the samples, or unless components other than KFMASH are present in quantities that are significant enough to affect the stabilities of the assemblages. The absence of carbonate minerals in the pelitic assemblages argues against significant CO_2 in the metamorphic fluid, though the $a(H_2O)$ of this fluid may have been locally variable.

Garnet either coexists with aluminosilicate + biotite in staurolite – absent assemblages, thus forming a three-AFM-phase assemblage, or occurs as an additional AFM phase, presumably stabilized by MnO. The T–X pseudo-sections suggest that garnet + aluminosilicate can only coexist in very Fe-rich bulk compositions in KFMASH, at similar temperatures to the stabilities of aluminosilicate + staurolite assemblages though additional components which preferentially stabilize garnet will expand the aluminosilicate – garnet stability fields at the expense of the other two-phase fields (see above). The P–T estimates may therefore be used to assess the total influence of a combination of the degree of disequilibrium and additional components to KFMASH on the phase relations in natural assemblages.

The P–T estimates and their errors were calculated by the program Thermocalc, using the default values for errors on the activity values for each end-member (see Powell 1985; Powell and Holland 1988; Holland and Powell 1990). These values are generally larger than the variation in activities calculated from mineral analyses from each assemblage. The activity values used in the P–T calculations were generated from the mineral analyses in Tables 1–4, using activity formulations after Powell and Holland (1990). Electron-probe analyses were taken from crystal rims; the only phase to show significant compositional zoning is garnet. The statistics

Table 5. Results from "Thermocalc" P–T calculations for selected pelitic assemblages

Number	Assemblage	T (°C)	P (kbar)
Average pressure – temperature calculations:			
185-636/4	bi + mu + st + gt + qz	583 ± 44	4.5 ± 1.0
281-215	bi + mu + st + gt + qz	649 + 44	5.1 ± 1.0
281-716	and + bi + mu + st + gt + qz	606 ± 42	4.6 ± 0.9
474-428	and + bi + mu + st + gt + qz	540 ± 40	3.8 ± 1.0
474-333	and + bi + mu + gt + qz	598 ± 52	4.3 ± 0.9
474-333a	and + bi + mu + gt + qz	602 ± 52	4.2 ± 0.9
474-333b	and + bi + mu + gt + qz	593 ± 52	4.4 ± 0.9

Average temperature calculations:			
Number	Assemblage	T (°C)	
		(4 kbar)	(4.5 kbar)
Andalusite-staurolite assemblages:			
185-716	and + bi + mu + st + qz	522 ± 24	549 ± 24
281-222	sill + bi + mu + st + gt + qz	578 ± 12	599 ± 12
281-223	and + bi + mu + st + gt + qz	570 ± 36	587 ± 36
281-715	and + bi + st + gt + qz	584 ± 8	606 ± 8
474-318	bi + mu + st + gt + qz	583 ± 8	604 ± 8
890-111	and + bi + mu + gt + qz	534 ± 107	553 ± 105
Temperature estimates generated from one independent reaction for each assemblage:			
185-440	gt + bt + mu + qz	564 ± 92	(4 kbar)

associated with the Thermocalc runs were often improved by removing the ferro-celadonite and Mg-staurolite end-members from the calculations despite the reduction in the number of independent relations needed to specify the P–T conditions for the assemblage. Thermocalc gave results using the average P–T calculations option for seven assemblages. In addition to these P–T pairs, Thermocalc generated temperature estimates for specified pressure values of 4 and 4.5 kbar for a further seven assemblages. The P–T estimates are listed in Table 5.

The average P–T values option of Thermocalc generated P–T conditions between 539 and 649° C and 3.8 and 5.1 kbar, most of these values lying between 583 and 606° C and 4.2 and 4.5 kbar. As a result, average temperatures were calculated at pressures of 4 and 4.5 kbar, giving values between 527 and 583° C at 4 kbar, and between 546 and 606° C at 4.5 kbar. Sample 890–111 occurred at lower grades than the other samples (Fig. 1), and its lower temperature, though the errors are large, is consistent with its lower metamorphic grade.

All the P–T and T–X pseudo-sections predict that andalusite- and/or staurolite-bearing assemblages should not be stable below ca. 560° C at 4 kbar or 570° C at 4.5 kbar. The temperature estimates at the appropriate pressures for these assemblages therefore tend to correspond closely to the stabilities predicted by the grids, though some temperature estimates are lower than these limits. These results imply that, in the Mount Lofty Ranges, components other than KFMASH have a relatively minor effect on the stabilities of aluminosilicate + staurolite + biotite. However, there are three garnet-bearing but staurolite-absent assemblages (therefore bearing 3 AFM phases) for which P–T estimates are available. Their estimated temperatures are similar to those of the other assemblages, but are ca. 50–100° C lower than the predicted stability limit for aluminosilicate + garnet + biotite assemblages in the KFMASH system. The garnets in these assemblages typically contain ca. 5–10 wt% MnO (Table 3). As illustrated above, significant MnO contents displace the aluminosilicate + garnet stability fields to lower temperatures and higher pressures than those predicted for the pure KFMASH system; presumably these measured Mn contents were enough to cause such a displacement in the Mount Lofty Ranges assemblages.

The P–T estimates vary over a relatively narrow range in values, not much larger than some of the calculated errors on the estimates, both within and between the three different areas from which the samples were collected. Importantly therefore these estimates indicate that the andalusite – staurolite and fibrolite zones throughout the Mount Lofty Ranges represent a restricted P–T range, and highlight the sensitivity of the pelitic system at these temperatures and pressures for bulk compositions in the vicinity of $X_{Fe} = 0.8$–0.7.

Discussion

In this study, we have calculated a P–T grid and accompanying pseudo-sections with an internally consistent data set and have compared these grids to natural occurrences of the assemblages concerned by assessing the ability of the grids and pseudo-sections to reproduce the prograde metamorphic zonation in the Mount Lofty Ranges. As described above, the pure KFMASH system cannot account for the presence of garnet + andalusite assemblages at similar grades to the aluminosilicate + staurolite assemblages. In addition, this system cannot account for the reaction texture described by Sandiford et al. (1990) in which staurolite is rimmed by cordierite during significant isobaric heating (as indicated by progressive replacement of kyanite then andalusite by sillimanite). However, it is possible to account for these observations qualitatively by assessing the likely consequences of additional components, known to be present in some phases in appreciable quantities.

The T–X_{Fe} pseudo-sections for reduced water activities (Fig. 6) show that variable fluid composition is likely to maintain the topologies of these pseudo-sections, hence preventing the growth of andalusite + chlorite down-grade of staurolite, which would otherwise result in the staurolite isograd occurring up-grade of the andalusite isograd. A possible alternative explanation for this reversal in isograds is that the zonal sequence represents an oblique profile through the terrain such that increases in metamorphic grade represent changes in pressure as well as temperature. Since the metamorphic field gradient is generally interpreted as the array of maximum-T conditions experienced by individual rocks exposed on the surface, it is unlikely that individual rock P–T paths approximate the P–T locus of this metamorphic field gradient (England and Richardson 1977). Sandiford et al. (1990) and Arnold and Sandiford (1991) have documented evidence that individual rocks from the Springton region have followed P–T paths involving isobaric heating. Figure 8 shows how a metamorphic field gradient with an andalusite + chlorite zone immediately down-grade of a staurolite + chlorite zone can be generated by an array of close-to-isobaric heating P–T paths. This field gradient is different at lower grades to that of the Scottish Stonehaven Sequence; this difference may explain the absence of well-defined garnet and chloritoid zones, which, according to Harte and Hudson (979) and Powell and Holland (1990) should occur immediately down-grade of the staurolite zone, but probably at slightly higher pressures than the lower grade parts of the metamorphic field gradient.

The curvature in the metamorphic field gradient inferred on the basis of local reversals in the "normal" isograd sequence in the Mount Lofty Ranges is consistent with the field exposures representing a slightly oblique section through a terrain in which heat was dissipated from intrusive bodies at discrete locations, a notion that is supported by considerably field evidence (Sandiford et al. 1990; Foden et al. 1990). In such an environment temperature gradients observed in the erosion surface must necessarily steepen towards the heat source and therefore surfaces that expose oblique sections with near-constant pressure gradient must necessarily give rise to metamorphic field gradients that are curved in P–T space.

Acknowledgements. This research was funded by the Australian Research Council as part of a study of heat- and mass-transfer processes at low pressures. Roger Powell is thanked for providing an unpublished version of Thermocalc used for the calculations presented herein, for many discussions concerning phase equilibria in metamorphic rocks and their graphical representation, and for comments on an earlier draft of the manuscript. Simon Harley and an anonymous reviewer provided comments that helped clarify some important points. We also thank P. Fleming for the loan of some thin sections and samples.

References

Arnold J, Sandiford M (1990) Petrogenesis of cordierite-orthoamphibole assemblages from the Springton region, South Australia. Contrib Mineral Petrol 106:100–109

Daily B, Milnes AR (1972) Significance of basal Cambrian metasediments of andalusite grade, Dudley Peninsula, Kangaroo Island, South Australia. Search 3:89–90

England P, Richardson SW (1977) The influence of erosion upon the mineral facies of rocks from different metamorphic environments. J Geol Soc Lond 134:201–213

Essene EJ (1989) The current status of thermobarometry in metamorphic rocks. In: Daly JS, Cliff RA, Yardley BWD (eds) Evolution of metamorphic belts: Geol Soc London Spec Publ 43, pp 1–44

Foden JD, Turner SP, Morrison G (1990) Tectonic implications of Delamarian magmatism in Sough Australia and Western Victoria. In: Jago JB, Moore PS (eds) The evolution of a late Precambrian-early Paleozoic rift complex: the Adelaide Geosyncline. Geol Soc Aust Spec Publ 16, pp 465–481

Glen RA, Laing WP, Parker AJ, Rutland RWR (1977) Tectonic relationships between the Proterozoic Gawler and Willyama orogenic domains, Australia. J Geol Soc Aust 24:125–150

Grew ES, Sandiford M (1985) Staurolite in a garnet-hornblende-biotite schist from the Lanterman range, northern Victoria Land, Antarctica. Neues Jahrb Miner Monatsh 9:396–410

Guidotti CV, Cheney JT, Conator PD (1975) Coexisting cordierite + biotite + chlorite from the Rumford Quadrangle, Maine. Geology 3:147–148

Guiraud M, Holland TJB, Powell R (1990) Mineral equilibria at glaucophane schist to eclogite facies in the system $Na_2O-MgO-FeO-Al_2O_3-SiO_2-H_2O$. Contrib Mineral Petrol 104:85–98

Harte B, Hudson NFC (1979) Pelite facies series and the temperatures and pressures of Dalradian metamorphism in E. Scotland. In: Harris AL, Holland CH, Leake BE (eds) The Caledonides of the British Isles – reviewed. Geol Soc Lond and Academic Press, Edinburgh, pp 323–337

Hensen BJ (1971) Theoretical phase relationships involving cordierite and garnet in the system $MgO-FeO-Al_2O_3-SiO_2$. Contrib Mineral Petrol 33:191–214

Hess PC (1969) The metamorphic paragenesis of cordierite in pelitic rocks. Contrib Mineral Petrol 63:175–198

Holdaway MJ, Lee SM (1977) Fe–Mg cordierite stability in high grade pelitic rocks based on experimental, theoretical and natural observations. Contrib Mineral Petrol 63:175–198

Holland TJB, Powell R (1990) An enlarged and updated internally consistent thermodynamic dataset with uncertainties and correlations: the system $K_2O-Na_2O-CaO-MgO-MnO-FeO-Al_2O_3-TiO_2-SiO_2-C-H_2-O_2$. J Metamorphic Geol 8:89–124

Hudson NFC (1980) Regional metamorphism of some Dalradian pelites in the Buchan area, N.E. Scotland. Contrib Mineral Petrol 73:39–51

Kerrick DM (1987) Fibrolite in contact aureoles of Donegal, Ireland. Am Mineral 72:240–254

Mancktelow NS (1990) The structure of the southern Adelaide Fold Belt, South Australia. In: Jago JB, Moore PS (eds) The evolution of a late Precambrian-early Paleozoic rift complex: the Adelaide Geosyncline. Geol Soc Aust Spec Publ 16, pp 369–395

Massonne HJ, Schreyer W (1987) Phengite geobarometry based on the limiting assemblage with k-feldspar, phlogopite and quartz. Contrib Mineral Petrol 96:212–224

Mills K (1964) The structural geology of an area east of Springton, South Australia. Unpubl PhD Thesis, Univ Adelaide

Milnes AR (1982) The Encounter Bay granites and their relationship to the Kanmantoo Group. In: Oliver RL, Gatehouse C (eds) Guide to excursions B1, B2, B3, B4, Geology of the Adelaide region. Fourth Int Symp Antarctic Earth Sci, pp 16–29

Miyashiro A, Shido F (1984) The Tschermak's substitution in low- and middle-grade pelitic schists. J Petrol 26:449–487

Offler R, Fleming PD (1968) A synthesis of folding and metamorphism in the Mt. Lofty Ranges, South Australia. J Geol Soc Aus 15:245–266

Pattison DRM (1987) Variations in Mg/(Mg + Fe), F, and (Fe,Mg)-Si = 2 Al in pelitic minerals in the Ballachulish thermal aureole, Scotland. Am Mineral 72:255–272

Powell R (1985) Geothermometry and geobarometry: a discussion. J Geol Soc Lond 142:29–38

Powell R, Evans JA (1983) A new geobarometer for the assemblage biotite-muscovite-chlorite-quartz. J Metamorphic Geol 1:331–336

Powell R, Holland TJB (1988) An internally consistent data set with uncertainties and correlations, 3: applications to geobarometry, worked examples and a computer program. J Metamorphic Geol 6:173–204

Powell R, Holland TJB (1990) Calculated mineral equilibria in the pelite system KFMASH ($K_2O-FeO-MgO-Al_2O_3-SiO_2-H_2O$). Am Mineral 75:367–380

Sandiford M, Oliver RL, Mills KJ, Allen RV (1990) A cordierite-staurolite association, east of Springton, Mt. Lofty Ranges: implications for the metamorphic evolution of the Kanmantoo Group. In: Jago JB, Moore PS (eds) The evolution of a late Precambrian – early Paleozoic rift complex: the Adelaide Geosyncline. Geol Soc Aust Spec Publ 16, pp 482–495

Seifert RC (1970) Low temperature compatibility relations of cordierite in haplopelites of the system $K_2O-MgO-Al_2O_3-SiO_2-H_2O$. J Petrol 11:73–99

Thompson AB (1976) Mineral reactions in some pelitic rocks, 11: calculation of some *P–T–X* (fe–Mg) phase relations. Am J Sci 276:425–454

Velde B (1965) Phengitic micas, synthesis, stability and natural occurrence. Am J Sci 263:886–913

Will T, Powell R, Holland TJB, Guiraud M (1990) Mineral equilibria at greenschist facies conditions in the system $CaO-MgO-FeO-Al_2O_3-SiO_2-H_2O-CO_2$. Contrib Mineral Petrol 105:347–358

Editorial responsibility: R. Binns